

Automated Segmentation of Brain Exterior in MR Images Driven by Empirical Procedures and Anatomical Knowledge

Andrew J. Worth, Nikos Makris, James W. Meyer, Verne S. Caviness, Jr.
and David N. Kennedy

Center for Morphometric Analysis, Neuroscience Center, Massachusetts General Hospital,
CNY-6, Building 149, 13th St., Charlestown, MA 02129-2000, USA.
<http://neuro-www.mgh.harvard.edu/cma/cma.homepage.html>
Email: andy@cma.mgh.harvard.edu

Abstract. This work demonstrates encouraging initial results for increasing the automation of a practical and precise MR brain image segmentation method. The intensity threshold for segmenting the brain exterior is automatically determined by locating the choroid plexus. This is done by finding peaks in a series of histograms taken over regions specified using anatomical knowledge. Intensity inhomogeneities are accounted for by adjusting the global intensity to match the white matter peak intensity in local regions. The results from 20 different brain scans (over 1000 images) obtained under different conditions are presented to validate the method which was able to determine the appropriate threshold in approximately 80% of the data.

1. Introduction

1.1. Significance

Magnetic resonance imaging provides a highly efficacious means for observing brain anatomy. Morphometric analysis provides quantitative measures of location, volume, shape and homogeneity of component brain structures. This type of analysis in conjunction with neuropsychological, neurological, and psychiatric observations and coupled with functional neuroimaging can then be used to aid in answering broad classes of questions about brain structure and function for both normal subjects and patient populations [1, 2]. For example, quantitative brain measurements have contributed to the study of developmental language disorders and autism [3], Alzheimer's disease [4-7], dyslexia [8, 9], attention deficit hyperactivity disorder [9-12], schizophrenia [13], multiple sclerosis [14, 15], Huntington's disease [16], and obsessive compulsive disorder [17].

Segmentation is the Bottleneck. In order to provide quantitative neuroanatomical measurements, the first step is to classify voxels as belonging to gray matter, white matter, cerebral spinal fluid (CSF), etc. and to delineate regions of these tissues in each brain slice image. The next step is to identify subregions as specific neuroanatomical structures. This task is difficult because it requires detailed anatomical knowledge and careful scrutiny of large amounts of data. This procedure accomplished manually is very tedious and therefore becomes prone to errors.

Segmentation is a bottleneck to further volumetric analysis [18], cerebral cortical subparcellation [19], and anatomic shape analysis [20].

While determination of absolute “accuracy” is problematic since there is no gold standard, there are many advantages of automating segmentation compared with performing the task manually. The main ones are: improved repeatability, improved reliability, and decreased variability. Results will be more repeatable because automated methods will always produce the same answer given the same data. Reliability will increase because errors that occur due to fatigue are eliminated. We have shown that inter-segmentor variability can decrease by automating the determination of thresholds while intra-segmentor reliability remains high [21]. Therefore consistency will improve both within and across morphometric studies. In addition to this, automatic routines act as a completely unbiased observer. Also, the availability of the analysis will increase since a computer program that can perform a given method is more portable and reproducible than a person. The decrease in human time necessary to perform a given segmentation task will allow a trade-off between the amount of time necessary for a study and the completeness of the morphometric analysis because more complete segmentations can be performed at the same cost. The use of automation can then lead to new classes of questions whereas previously the time commitment would have been prohibitive.

1.2. Task Definition

Much of the MR brain segmentation research focuses on assigning voxels to gray matter, white matter, and CSF classes. While this can be sufficient for applications such as 3D visualization, it is not adequate for undertaking *quantitative* neuroanatomical studies which hope to uncover correlations between brain structure and function or disease. Beyond classifying each voxel in the entire brain scan, a specific label must be assigned to the voxel regions that represent the corresponding neuroanatomical structure. Furthermore, it can be desirable to subdivide these structures and even to parcellate gray matter and white matter into meaningful units [19]. Also, each structure has its own specific problems arising from its characteristic intensities, shape, position, and its neighboring structures. A *complete* segmentation is desirable because it is not always clear which neuroanatomical structures may be of interest in advance. For instance, Filipek et al. segment cortical gray matter, subcortical white matter, lateral, third and fourth ventricles, caudate, putamen, globus pallidus, hippocampus-amygdala complex, thalamus, brainstem, cerebellum cortex and cerebellar central mass [22].

In order to produce statistically significant results, the segmentation boundary in the image must precisely represent the boundary of the anatomical structure even if the information present in the image is corrupted or missing. Since practical MR image data often comes from a variety of sources and has variable scan quality, the procedures which convert raw image data into useful statistics must be robust. They must also be reliable enough to allow the quantitative comparison of brain volumes across multiple studies. And finally, the entire procedure must use only a reasonable amount of time and effort.

These constraints pose significant difficulties for the currently available methods to satisfy without human intervention. Therefore, while the ultimate goal is completely automatic MR brain segmentation, the interim and more practical goal of the research described here is to increase reliability and repeatability while decreasing

variability and cost. We seek to automate the segmentation and identification tasks which are necessary to precisely measure neuroanatomical structures of interest. In this paper, the specific structure of interest is the exterior of the brain.

1.3. Previous and Related Work

There is currently no completely automatic method for segmenting a given neuroanatomical structure or even separating gray and white matter that has been shown to work with the precision of a human expert on large numbers of brain scans. For surveys on segmentation of brain images, see [23-26]. For a general image processing reference (and specifically for finding peaks in histograms as described below) see [27].

There are many descriptions of manual or semi-automatic methods in the literature (for a survey involving schizophrenia, see [28]). Some recent work includes [11, 29-31]. While there are no completely automatic methods which can precisely segment a complete set of specific neuroanatomical structures, there are a number of recent techniques that provide solutions and produce good results for specific problems [32-39]. Due to its cost in time and effort, many demonstrations are presented in the literature but a thorough validation is rarely performed. In this work, we attempt to present favorable results using a significant amount of practical data.

2. Method

2.1. Overview

This paper focuses on increasing the automation of segmentation of the exterior of the brain. In the sections below, we describe the currently established segmentation method, the techniques developed to automate part of the segmentation task, and finally, how the automated results are incorporated into the segmentation method. The remaining sections in the paper describe and discuss the results of applying this method to 20 test brains.

2.2. Positional Normalization and Cropping

In studies performed at the Center for Morphometric Analysis, coronal T1-weighted volumetric MR scans are used because they provide good contrast for the visualization of brain anatomy. The first step in their quantitative analysis is to normalize the position of the brain in 3D. This is done by trained experts who reposition the scan using the midpoints of the decussations of the anterior and posterior commissures ("AC" & "PC") and the midsagittal plane at the level of posterior commissure. The repositioned scans are then resliced into a normalized coronal scan which is used for subsequent analyses. This translation and rotation places the brain in the orientation of the Talairach coordinate system [40, 41].

The next step is to manually crop the normalized scan. In this step, the slice range where brain tissues are seen is determined by examining representative coronal and sagittal images. The horizontal and vertical extents of the brain are also determined using these images. All data outside of these locations are ignored and subsequent analysis is performed on the cropped and positionally normalized data.

2.3. Established Segmentation Method

The goal of this paper is to automate part of the general semi-automated segmentation method which has already been established. This method involves a skilled operator using a computer program to produce outlines around each neuroanatomical structure of interest by choosing appropriate iso-intensity contours and making manual refinements and corrections [18, 22]. Corrections can become necessary when the data is too noisy, has low contrast, is skewed by intensity gradients, has extensive partial volume voxels (when a voxel includes multiple tissue types resulting in an intermediate intensity), or because part of the structure is too small to make a sufficient appearance. Moreover, manual drawing is always necessary when there is no contrast difference between neuroanatomical structures because they are composed of similar tissues.

Specifically, we seek to automate the segmentation of the exterior boundary of the brain. This border is defined as the outermost edge of the cortex that underlies the pia mater. This boundary should include all gray matter and exclude all dura mater, meninges, and other cerebral extra-cerebral CSF and tissues. The optic chiasm is also considered to be outside of the brain. The expert segmentor produces outlines for the cerebral exteriors using iso-intensity contours in the coronal view. However, sagittal and axial views are also inspected to resolve spatial ambiguities regarding the extent of the brain. First the screen is brightened so that the low range of intensities becomes visible. An intensity value is chosen such that the iso-intensity contour produced is definitely outside of the brain. Then, the intensity is increased to “tighten” the outline around the hemispheres. Lastly, meninges and connections with other tissues must be removed by manually drawing outlines that exclude them from the final exterior outline. Each cerebral hemisphere is extracted independently. When corpus callosum is present, it is necessary to separate the hemispheres by manually drawing along the midline. At the frontal-temporal junction, if the contour encompasses the entire hemisphere, but the white matter between the lobes is not continuous, it is necessary to separate them as well.

After segmentation, the final step in a quantitative brain volume study is to calculate the volumes of the structures of interest. This is done by counting the number of voxels that belong to each structure as prescribed by the outlines. The outline voxels themselves are considered to belong half inside and half outside of the structure.

2.4. Rationale: Choroid Plexus Indicates Brain Exterior Threshold

The method described above involves many different judgments by the segmentor. The most significant is the determination of the intensity threshold which defines the majority of the outline – i.e. how “tight” to make the exterior border around the brain. To automate this decision, we base our method on the observation (described in an unpublished report [42]) that since the choroid plexus is composed of tissues and fluids which are similar to those found in the subarachnoid space (dura and pia mater, vessels, and cerebral spinal fluid), the MR signal intensity should also be similar. Figure 1 shows the choroid plexus as it appears in a T1-weighted coronal slice. Since the subarachnoid space separates the exterior of the brain from the exterior CSF and since this area should have an MR intensity that is between CSF and gray matter, a border may be placed at this location using an iso-intensity contour



Fig. 1: Choroid plexus (circled) as seen in a coronal T1 MR image.

defined by the intensity of the choroid plexus. However, because there is usually a drift in intensity both between and across slices, this threshold must be adjusted for each local slice region. The next section describes the series of automatic procedures necessary to determine the intensity of the choroid plexus and how this intensity is locally adapted for use in each slice.

2.5. Determination of Automated Exterior Threshold

Before it is possible to determine the intensity of the choroid plexus, approximate global thresholds for gray matter, white matter, and CSF must be determined. This is done by finding the peaks in a histogram of the entire brain. After classifying all voxels using global thresholds determined using the peaks, a histogram of the ventricles is taken so that accurate thresholds may be determined within the CSF. The new thresholds allow a more accurate classification of voxels, and a second histogram taken over CSF voxels finally contains a peak for the choroid plexus. These steps are now described in detail.

Take Global Histogram. In order to get a general idea of the intensity values for gray matter, white matter and CSF, a histogram is taken over the intracranial region defined by a series of boxes accounting for Talairach atlas sections “B” through “H” which are completely inside the skull [40]. Only the data in these “intracranial boxes” is considered so that when a histogram is taken, it will represent primarily brain tissues and CSF and will not be influenced by other non-brain tissues with similar intensities. This atlas technique is accurate enough for the central brain regions and it is only necessary that *most* of the non-brain intensities be excluded so that they do not have a significant effect on determining the peaks in the histogram. To emphasize the homogeneous tissue intensities, voxels that are part of strong edges are excluded (as measured by their Sobel edge magnitude, see [27]).

Find Peaks in Histogram. The derivative of the histogram is taken by convolving it with the derivative of a Gaussian and then the peaks are found by locating negative-going zero crossings. Very small peaks in the original histogram do not survive in the derivative of the histogram (the derivative never actually goes below zero) since the derivative of a Gaussian convolution kernel also smoothes the result by an amount that depends on the standard deviation of the Gaussian. This

standard deviation is determined from the width of the histogram; it is calculated as 0.04 times the difference between the intensities at 10% and 90% of the cumulative histogram. Other slightly larger peaks are ignored if their area is less than 1/30th of the total area of the histogram. This incorporates *a priori* knowledge about the occurrence of these primary tissues of interest.

The method for determining intensity model parameters using histograms and their derivatives works well even for a wide variety of brain scan data sets obtained at different times from different scanners under different protocols: in an initial study, the correct peaks were identified in a representative slice in 59 out of 79 brains scans attempted and the failures occurred in very noisy and large intensity gradient data which was far worse than the data used in the current study [21].

Set Global Thresholds and Label Voxels. After finding the peaks in the histogram, the lowest intensity peak is assumed to be CSF, the second to highest peak is gray, and that the highest peak found is white matter. Next, the gray-white and CSF-white matter thresholds are calculated by taking the intensity midway between their respective peaks:

$$CSFG_{thresh} = (CSF_{mean} + WM_{mean})/2,$$

$$GW_{thresh} = (GM_{mean} + WM_{mean})/2.$$

This “mid-peak histogram method” was devised because the regions over which histograms are taken are often too small to provide significant estimates of the variances of the tissue intensities. Using only the peaks makes the procedure repeatable and robust.

The next step is to use these global thresholds to classify each voxel in the whole data set as belonging to the following classes: “CSF”, “gray”, “white”, and “other”.

Find Real CSF peaks, Calculate New Thresholds, Reclassify Voxels.

Next, a histogram is taken over only those voxels which are classified as CSF. Also, by defining a box around the center of the brain, only ventricle CSF will be included in this histogram. This box is defined to be half of the horizontal width of the cropped data (in the coronal view) and vertically extends from the level of the anterior commissure (AC) to one third of the distance between the AC and the top of the brain. Only the coronal slices between and including the AC and posterior commissure (PC) are in this box to minimally include CSF-gray partial volume voxels (since the main axes of the lateral ventricles in these slices are perpendicular to the coronal plane). Peaks are found in this histogram as was done previously and again CSF is assumed to be the lowest intensity peak. A new CSF threshold is calculated to be midway between this new CSF peak and the previously determined gray peak. This new threshold allows a more accurate classification of every voxel.

Find Choroid Plexus Intensity. With this new voxel classification, a more accurate histogram can be taken over CSF voxels in the ventricle box (defined above). This histogram should include choroid plexus because choroid plexus is found inside the ventricles at an intensity that is between CSF and gray matter but closer to CSF intensities. The last (highest intensity) peak found in this histogram (using the previously described zero-crossing method) is assumed to represent choroid plexus intensities. This intensity value is the desired global value for defining isointensity contours to outline the brain exterior. Figure 2 shows an example of the peaks and histogram after this step. The small bump in the middle of the histogram in Figure 2

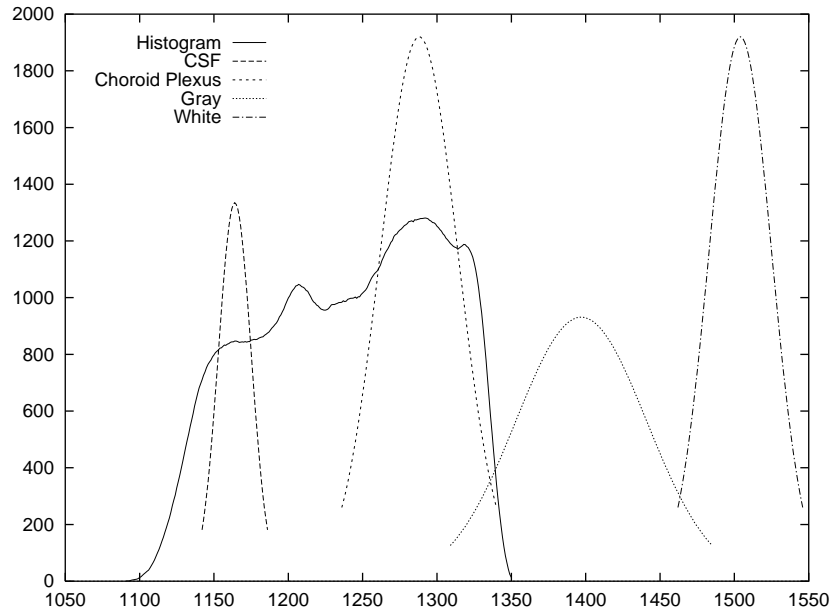


Fig. 2: Plot showing a smoothed histogram taken over voxels classified as CSF in the ventricle region. The 4 peaks shown correspond (from left to right) to ventricle CSF, choroid plexus, gray matter, and white matter. Peaks heights are arbitrary. The gray and white peaks were obtained from an earlier histogram (not shown).

is ignored since it is the highest intensity peak in the ventricle histogram that corresponds to choroid plexus.

Adjust Global Exterior Intensity for Each Slice. Due to intensity drift in the image data, the global intensity which defines the cerebral exterior outline must be adjusted in each half of the brain in each slice. This is done by locally finding the white matter peak in this region of each slice. First, the brain region is located by finding the largest connected region of voxels classified as “gray” and “white” that is in the middle of the left (or right) half of the image. Peaks are found in a histogram taken over this brain region and the highest intensity peak is assumed to be white matter. The local threshold for the brain exterior is calculated as:

$$l_{Exterior} = \frac{(g_{Exterior} - g_{CSF})}{(gW - g_{CSF})} \times (lW - g_{CSF}) + g_{CSF},$$

where “l” means local and “g” means global. The result is a threshold that can be used to segment the exterior of the brain. If there were any problems (i.e. if no local white matter peak could be found), then the global threshold is used. The “localness” of this calculation can range from one threshold per slice to a continuous field of thresholds (one for each voxel).

2.6. Incorporation of Automated Results

The intensity threshold results are provided to the segmentor as the first step towards segmenting each slice. The threshold is available as a button which generates intensity contours over the entire slice at that intensity. The segmentor then incorporates this pre-calculated intensity contour into the normal segmentation method. If the pre-calculated thresholds are accurate, this saves time because it obviates the need to pick an intensity and adjust it by hand. However, the automated threshold provides no assistance where the boundary needs to be hand-drawn or if the pre-calculated threshold is incorrect.

3. Results

3.1. Data

The coronal MR brain slice images in this study are obtained using T1-weighted “spoiled GRASS” (SPGR, GE MRI Systems), “FLASH” or “MP-RAGE” (Siemens MRI Systems) images. The segmentation task becomes easier with increasing scan quality and resolution, and by using multispectral images [26]. However, we focus on segmentation using only a single structural image because this data provides a good balance between contrast, spatial resolution, and scanning time, and is routinely available. Furthermore, since the problem is defined as the detailed segmentation of specific neuroanatomical structures, the difficulties which we overcome here are still important when using less noisy and multispectral data.

Scans were typically acquired at the NMR Center of the Massachusetts General Hospital with a 1.5 Tesla General Electric Signa. Contiguous 3.0 mm three-dimensional coronal T1-weighted SPGR images of the entire brain were attained with the following parameters: TR = 50 msec, TE = 9 msec, flip angle = 50 degrees, field of view = 24 cm., matrix = 256x256, and averages = 1. Some scans were acquired using a similar protocol at the McLean Hospital. The scans were taken of twelve females and eight males who were roughly divided between controls and patients. The patients were diagnosed with obsessive compulsive disorder, Trichotillomania, schizophrenia, or with stroke.

Figure 3 shows an example of using the automated threshold to segment the brain exterior. The initial outlines produced with this threshold (b) must usually be edited to obtain the desired final outline (c). This manual drawing can be to add a boundary that is not present (e.g. the right/left division), remove meninges (e.g. at the upper right of the slice), or possibly to include some brain material that was missed (not shown).

3.2. Complete Evaluation of One Brain

In order to evaluate the effectiveness of the automatic threshold determination method, the exterior was segmented in a single brain with and without using the automated threshold. After the global thresholds were determined, only one local threshold was calculated for each slice, and this was taken over only the right half of the image (the left half of the brain) to explore the sensitivity of this method to gradients within each slice. The resulting average overlap (number of pixels in both outlines divided by 1/2 the sum of the number of pixels in each) was measured to be 94% and 93% for

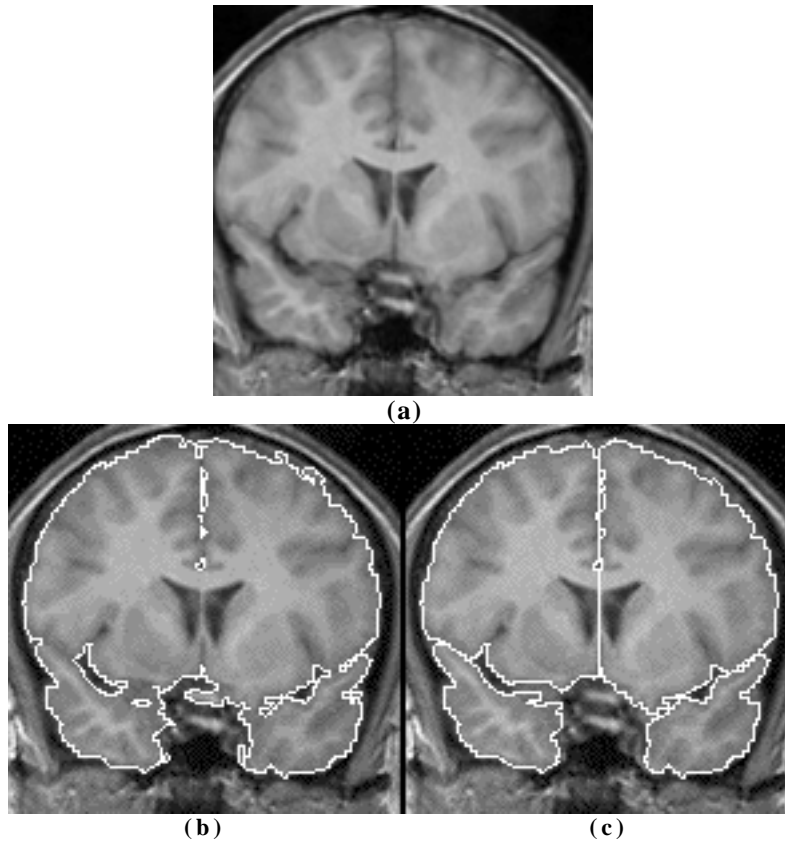


Fig. 3: Example Results. The raw image (a) the outlines produced using the resulting threshold (b), and the final image after being edited by the expert segmentor (c).

the left and right exteriors (respectively). This indicates that the segmentor performed basically the same segmentation with and without using the automated threshold and that there was little effect of left-to-right gradients within the slices. The amount of time necessary for segmenting without the automatic threshold was 91 minutes and 73 minutes when using the automated threshold. This is a time savings of about 20%.

3.3. Appraisal of 20 Brains

After the complete segmentation of one brain scan, it became clear that the other scans had similar results. In order to save time by not performing the complete segmentation, 20 scans were evaluated by estimating the number of changes that would be needed to finish the segmentation. This was done by giving two scores for each brain: the percentage of slices where the intensity was correctly chosen, and (in these slices) the percentage of the outlines that were useful. Using all 20 scans, the intensity threshold was correctly chosen for approximately 80% of the images. Because hand drawing needs to be done in most slices (as can be seen in Figure 3

above) the outlines in each slice are approximately 80-95% useful. By multiplying the usefulness of each correctly thresholded slice by the percentage of useful slices in each scan, and by assuming that the image slices where the threshold was *not* chosen correctly contain no useful outlines (which is not the case), in the 20 scans we obtained an average “usefulness” of 74%. In fact, many of the scans where the threshold was slightly miscalculated do contain useful outline information, so this number is slightly low.

Three of the scans had intensity thresholds chosen correctly for every slice image. In the majority of the other scans, around 95% of the outlines were correct using the automatic threshold and a few scans were as low as 16% correct. The worst scan had a large intensity gradient. Most of the errors occurred at the anterior and posterior slice extremes. This is understandable since the method adapts the local threshold to the white matter peak which becomes increasingly effected by partial volume as the folds of the cortex pass in and out of the slice acquisition plane in the extreme slices.

A number of brain scans were not able to be segmented at all by this method because the algorithm was not able to determine the location of the initial global peaks. This occurred in very noisy data with large intensity inhomogeneities or in data where there was very little grey-white contrast (i.e. these two peaks began to merge together). A numerical measurement of how close the automatic threshold comes to the intensity chosen by the expert segmentor presents difficulties due to the hand drawing which is usually necessary. It is also not clear that the expert segmentor’s result should always be treated as the correct answer since that segmentor’s state of alertness and amount of training is unknown.

4. Discussion

Theoretically driven approaches found in the literature can claim to segment MR brain images fully automatically only if they solve a less demanding problem than the one defined herein. No method can be used for precise segmentation unless it adequately deals with, among other things: parameter estimation, missing boundary completion, partial voluming, and intensity inhomogeneities. These problems may not fit well into the theoretical formalism or else they may make the method intractable. As an alternative to such theoretically-driven approaches, we pursue the more empirical direction taken in the present work. We seek to directly address the most significant problems by incorporating as much available information as is necessary (as have, for instance [38, 39, 43, 44]). This brute force or *ad hoc* strategy usually results in solutions that are detailed, complicated and thereby difficult to understand and evaluate. The only certain way to judge the effectiveness of any approach is by the results, and therefore a thorough validation is necessary even lacking a true “gold standard”. Our emphasis here is to automate an established, precise segmentation procedure and not to develop abstract segmentation methods.

However, we also seek to encourage the development of rigorous ways of flexibly incorporating various kinds of information for segmentation. Since one of the fundamental problems of all image segmentation methods is to continue to produce acceptable results as problems become more demanding, the utility of this paper to the general image processing community is to add evidence for the importance of dealing directly with problems by using deep domain specific knowledge. This paper provides an example of the application of *structural knowledge* (expectations about tissue response in MR such as histogram peak sizes and knowing which peak to use

in which situation; templates located relative to landmarks such as the intracranial boxes and knowing where to find the choroid plexus), and *procedural knowledge* (specific sequence of successive region of interest refinements), along with image processing and pattern recognition methods (locating peaks using the derivative of a Gaussian; and excluding edge voxels from influencing threshold determination).

5. Conclusion

Semi-automated methods are currently the only way to perform a complete volumetric analysis and (with the appropriate controls and testing) are the only way to insure that the segmentation boundary in the image precisely represents the boundary of the anatomical structure of interest. This is due to the following reasons: practical MR image data often comes from a variety of sources and has variable scan quality; the information which should be in the scan is often corrupted or missing; painstaking, precise segmentation of MR images requires a lot of time and effort; a great deal of scans are needed to make a study's result significant; and also that completely automatic approaches have not yet been shown to produce sufficiently accurate segmentation results in all situations.

We have contributed to the automation of MR brain segmentation by demonstrating an improvement to an existing method for undertaking quantitative neurological studies using MR images. The methods presented in this paper provide an automatic determination of thresholds to segment the exterior of the brain in MR images. We will continue this effort by determining region shapes (such as the intracranial boxes mentioned above) and parameter settings from previously segmented brain data sets. We will also extend this method to other neuroanatomical structures and will combine the entire package in a system which will produce precise, reliable results with minimal human intervention.

Acknowledgment This work was supported in part by grant NS 27950 and NS 34189 from the National Institute of Neurologic Disorders and Stroke and also in part by the Fairway Trust. We thank the anonymous reviewers for their helpful comments. The authors would also like to thank Julie M. Goodman, Elizabeth A. Hoge, Mark R. Patti, Jason A. Tourville, Jill M. Goldstien, Larry J. Sideman, and Pauline A. Filipek for their valuable contributions to the segmentation methods described herein.

References

1. V. S. Caviness, Jr., P. A. Filipek, and D. N. Kennedy, "Magnetic resonance technology in human brain science: A blueprint for a program based upon morphometry," *Brain Dev.*, vol. 11, pp. 1-13, 1989.
2. V. S. Caviness, Jr., P. A. Filipek, and D. N. Kennedy, "Quantitative magnetic resonance imaging and studies of degenerative diseases of the developing human brain," *Brain-Dev.*, no. 14 Suppl, pp. S80-5, 1992.
3. P. Filipek, C. Richelme, D. Kennedy, J. Rademacher, D. Pitcher, S. Zidel, and V. C. Jr., "Morphometric analysis of the brain in developmental language disorders and autism," *Ann Neurol.*, vol. 32, p. 475, 1992.

4. M. Ashtari, J. Zito, B. Gold, J. Lieberman, Borenstein, and P. Herman, "Computerized volume measurement of brain structure," *Invest Rad*, vol. 25, pp. 798-805, 1990.
5. C. Jack, F. Sharbrough, C. Twomey, G. Cascino, K. Hirschorn, W. Marsh, A. Zinsmeister, and B. Scheithaure, "Temporal Lobe Seizures: Lateralization with MR Volume Measurements of the Hippocampal Formation," *Radiology*, pp. 423-429, 1990.
6. P. Scheltens, D. Leys, F. Barkhof, and e. al., "Atrophy of the medial temporal lobes on MRI in probable Alzheimer's disease and normal ageing: Diagnostic value and neuropsychological correlates," *J. Neurol Neurosurg Psychiatry*, vol. 55, pp. 967-72, 1992.
7. J. Seab, W. Jagust, S. Wong, M. Roos, B. Reed, and T. Budinger, "Quantitative NMR measurements of hippocampal in Alzheimer's disease," *Mag Res Med*, vol. 8, pp. 200-8, 1988.
8. R. Duara, A. Kushch, K. Gross-Glen, and e. al., "Neuroanatomic differences between dyslexic and normal readers on MRI scans," *Arch Neurol*, vol. 48, pp. 410-16, 1991.
9. G. Hynd, M. Semrud-Clikeman, A. Lorys, and e. al., "Brain morphology in developmental dyslexia and attention deficit disorder," *Arch Neurol*, vol. 47, pp. 919-26, 1990.
10. G. Hynd, M. Semrud-Clikeman, A. Lorys, and e. al., "Corpus callosum morphology in attention deficit disorder (ADHD): Morphometric analysis of MRI," *J Learn Disab*, vol. 24, pp. 121-46, 1991.
11. F. X. Castellanos, J. N. Giedd, W. L. Marsh, S. D. Hamburger, A. C. Vaituzis, D. P. Dickstein, S. E. Sarfatti, Y. C. Vauss, J. W. Snell, N. Lange, D. Kaysen, A. L. Krain, G. F. Ritchie, J. C. Rajapakse, and J. L. Rapoport, "Quantitative brain magnetic resonance imaging in attention-deficit hyperactivity disorder," *Archives of General Psychiatry*, vol. 53, pp. 607-616, 1996.
12. P. A. Filipek, M. Semrud-Clikeman, R. J. Steingard, P. F. Renshaw, D. N. Kennedy, and J. Biederman, "Volumetric MRI Analysis Comparing Attention-Deficit Hyperactivity Disorder and Normal Controls," *Annals of Neurology*, in press.
13. M. E. Shenton, R. Kikinis, F. A. Jolesz, S. D. Pollak, M. LeMay, C. G. Wible, H. Hokama, J. Martin, D. Metcalf, M. Coleman, and et al., "Abnormalities of the left temporal lobe and thought disorder in schizophrenia," *N-Engl-J-Med.*, vol. 327, no. 9, pp. 604-12, 1992.
14. D. Wicks, P. Tofts, D. Miller, and e. al., "Volume measurement of multiple sclerosis lesions with magnetic resonance images: A preliminary study," *Neuroradiology*, vol. 34, pp. 475-9, 1992.
15. J. Simon, R. Schiffer, R. Rudick, and R. Herndon, "Quantitative determination of MS-induced corpus callosum atrophy in vivo using MR imaging," *AJNR*, vol. 8, pp. 599-604, 1987.
16. G. J. Harris, G. D. Pearlson, C. E. Peyser, E. H. Aylward, J. Roberts, P. E. Barta, G. A. Chase, and S. E. Folstein, "Putamen volume reduction on magnetic resonance imaging exceeds caudate changes in mild Huntington's disease," *Ann-Neurol.*, vol. 31, no. 1, pp. 69-75, 1992.

17. H. Breiter, P. Filipek, D. Kennedy, and e. al., "Pronounced white matter abnormalities in patients with obsessive compulsive disorder," in *Paper presented at Boston Society of Neurology and Psychiatry*, 1992, .
18. D. N. Kennedy, P. A. Filipek, and V. S. Caviness, Jr., "Anatomic segmentation and volumetric calculations in nuclear magnetic resonance imaging," *IEEE Transactions on Medical Imaging*, vol. 8, no. 1, pp. 1-7, 1989.
19. J. Rademacher, A. Galaburda, D. Kennedy, P. Filipek, and V. C. Jr., "Human cerebral cortex: Localization, parcellation and morphometry with magnetic resonance imaging," *J Cog Neurosci.*, vol. 4, pp. 352-74, 1992.
20. D. Kennedy, P. Filipek, and V. C. Jr., "Fourier shape analysis of anatomic structures," in *Recent Advances in Fourier Analysis and its Applicaitons, NATO ASI Series*. Dordrecht, The Netherlands: Kluwer Academic Publishers, 1990, pp. 17-287.
21. A. J. Worth, N. Makris, M. R. Patti, J. M. Goodman, E. A. Hoge, V. S. Caviness, Jr. , and D. N. Kennedy, "Precise Segmentation of the Lateral Ventricles and Caudate Nucleus in MR Brain Images using Anatomically Driven Histograms," *IEEE Transactions on Medical Imaging*, (submitted).
22. P. A. Filipek, C. Richelme, D. N. Kennedy, and V. S. Caviness, Jr., "The young adult human brain: an MRI-based morphometric analysis," *Cereb-Cortex.*, vol. 4, no. 4, pp. 344-60, 1994.
23. L. O. Hall, A. M. Bensaid, L. P. Clarke, R. P. Velthuizen, M. S. Silbiger, and J. C. Bezdek, "A comparison of neural network and fuzzy clustering techniques in segmenting magnetic resonance images of the brain," *IEEE Transactions on Neural Networks*, vol. 3, no. 5, pp. 672-82, 1992.
24. J. C. Bezdek, L. O. Hall, and L. P. Clarke, "Review of MR image segmentation techniques using pattern recognition," *Medical Physics*, vol. 20, no. 4, pp. 1033-1048, 1993.
25. A. P. Zijdenbos and B. M. Dawant, "Brain segmentation and white matter lesion detection in MR images," *Critical Reviews in Biomedical Engineering*, vol. 22, no. 5-6, pp. 401-65, 1994.
26. L. P. Clarke, R. P. Velthuizen, M. A. Camacho, J. J. Heine, M. Vaidyanathan, L. O. Hall, R. W. Thatcher, and M. L. Silbiger, "MRI segmentation: Methods and applications," *Magnetic Resonance Imaging*, vol. 13, no. 3, pp. 343-368, 1995.
27. J. C. Russ, *The image processing handbook*, 2nd ed. Boca Raton, Florida: CRC Press, Inc., 1995.
28. S. Chua and P. McKenna, "Schizophrenia – a Brain Disease? A Critical Review of Structural and Functional Cerebral Abnormality in the Disorder," *British Journal of Psychiatry*, vol. 166, pp. 563-582, 1995.
29. R. G. Petty, P. E. Barta, G. D. Perlson, I. K. McGilcrist, R. W. Lewis, A. Y. Tien, A. Pulver, D. D. Vaughn, M. F. Casanova, and R. E. Powers, "Reversal of Asymmetry of the Planum Temporale in Schizophrenia," *American Journal of Psychiatry*, vol. 152, no. 5, pp. 715-721, 1995.
30. M. S. Buchsbaum, T. Someya, C. Y. Teng, L. Abel, S. Chin, A. Najafi, R. J. Haier, J. We, and W. E. Bunney, "PET and MRI of the Thalamus in Never-Medicated Patients with Schizophrenia," *American Journal of Psychiatry*, vol. 153, no. 2, p. 191-199, 1996.

31. J. N. Giedd, J. W. Snell, N. Lange, J. C. Rajapakse, B. J. Casey, P. L. Kozuch, A. C. Vaituzis, Y. C. Vauss, S. D. Hamburger, D. Kaysen, and J. L. Rapoport, "Quantative Magnetic Resonance Imaging of Human Brain Development: Ages 4-18," *Cerebral Cortex*, vol. 6, pp. 1047-3211, 1996.
32. A. P. Zijdenbos, B. M. Dawant, and R. A. Margolin, "Inter- and Intra-Slice Intensity Correction in MR Images," *Proc Information Processing in Medical Imaging*, vol. 14, pp. 349-350, 1995.
33. P. H. Bland and C. R. Meyer, "Robust three-dimensional object definition in CT and MRI," *Medical Physics*, vol. 23, no. 1, pp. 99-107, 1996.
34. W. M. Wells, W. E. L. Grimson, R. Kikinis, and F. A. Jolesz, "Adaptive Segmentation of MRI Data," *IEEE Transactions on Medical Imaging*, vol. 15, no. 4, pp. 429-442, 1996.
35. J. C. Rajapakse, J. N. Giedd, and J. L. Rapoport, "Statistical approach to segmentation of single-channel cerebral MR images," *IEEE Transactions on Medical Imaging*, (in press).
36. E. A. Ashton, M. J. Berg, K. J. Parker, J. Weisberg, C. Chang Wen, and L. Ketonen, "Segmentation and feature extraction techniques, with applications to MRI head studies," *Magnetic Resonance in Medicine*, vol. 33, no. 5, pp. 670-7, 1995.
37. A. Lundervold and G. Storvik, "Segmentation of brain parenchyma and cerebrospinal fluid in multispectral magnetic resonance images," *IEEE Transactions on Medical Imaging*, vol. 14, no. 2, pp. 339-349, 1995.
38. C. Tsai, B. S. Manjunath, and R. Jagadeesan, "Automated segmentation of brain MR images," *Pattern Recognition*, vol. 28, no. 12, pp. 1825-37, 1995.
39. M. Sonka, S. K. Tadikonda, and S. M. Collins, "Knowledge-Based Interpretation of MR Brain Images," *IEEE Transactions on Medical Imaging*, vol. 15, no. 4, pp. 443-452, 1996.
40. J. Talairach and P. Tournoux, *Co-Planar Stereotaxic Atlas of the Human Brain*: New York: Thieme Medical Publishers, Inc., 1988.
41. P. Filipek, D. Kennedy, and V. Caviness, "Volumetric analysis of central nervous system neoplasms based on MRI," *Pediatric Neurology*, vol. 7, pp. 347-51, 1991.
42. N. Makris, "Theoretical segmentation mechanism for identifying periventricular structures in the human central nervous system," Boston University, Department of Biomedical Engineering, BE 515 Term Paper, Boston, MA, (unpublished report) Spring 1995.
43. M. E. Brummer, R. M. Mersereau, R. L. Eisner, and R. R. J. Lewine, "Automatic detection of brain contours in MRI data sets," *IEEE Transactions on Medical Imaging*, vol. 12, no. 2, pp. 153-66, 1993.
44. A. J. Worth and D. N. Kennedy, "Segmentation of magnetic resonance brain images using analogue constraint satisfaction neural networks," *Image and Vision Computing*, vol. 12, no. 6, pp. 345-354, 1994.